Submitted to Applied Clay Science

Using Ca-Fe layered double hydroxide transformation to optimise phosphate removal from waste waters

Muayad Al Jaberi[a], Martine Mallet[a], H. Chris Greenwell[b], Mustapha Abdelmoula[a] and Christian Ruby[a,*]

[a]Laboratoire de Chimie Physique et Microbiologie pour les Matériaux et l'Environnement, LCPME UMR 7564 CNRS-Université de Lorraine, 405 rue de Vandoeuvre 54600 Villers-lès-Nancy, France.

[b]Department of Earth Sciences, Durham University, South Road, Durham DH1 3LE, UK.

[*] Corresponding author: Christian.ruby@univ-lorraine.fr

Postal address: LCPME, 405 rue de Vandoeuvre 54600 Villers-lès-Nancy, France.

Abstract

Single phase Ca-Fe layered double hydroxide (LDH) minerals containing Cl^- species in the interlayer was synthesised by coprecipitation with a Ca^{II} : Fe^{III} ratio of 2 : 1. In both phosphate (PO_4) free water and at low aqueous PO_4 concentration, the LDH was fully transformed into a mixture of a "ferrihydrite-like" material, calcite and soluble calcium species. Mössbauer spectroscopy and transmission electron microscopy showed that phosphate was removed by the "ferrihydrite like" phase that contained a significant quantity of Ca. At high phosphate concentration the Ca species released from the LDH precipitated to form hydroxyapatite leading to a maximal removal capacity of ~ 130 mg P-PO_4 g^{-1}. The Ca-Fe LDH was deposited onto a pozzolana volcanic rock in order to perform a column experiment under hydrodynamic conditions for 70 days. A high removal capacity was

observed, a q_B of ~ 4 mg P-PO_4 g^{-1} was measured at the breakthrough of the column, however the pH in the outflow was measured to be higher than 11. Such an increase was due to the very high solubility of the Ca-Fe LDH.

Keywords : LDH; Iron; Water treatment; Adsorption; Precipitation; Hydroxyapatite

1. Introduction

Protection and monitoring of water resources are among the major issues of the twenty-first century due to population growth, rapid industrialization and intensification of agriculture. Among the various pollutants that threaten water quality, orthophosphate species ($H_{3-x}PO_4^{x-}$ subsequently named PO_4) are of utmost importance since the excess of PO_4 is mainly responsible for the phenomena of water eutrophication. Eutrophication leads to strong perturbation of biodiversity and important economic losses, *e.g.* closing of fisheries and groundwater production wells. As an example, an annual cost of € 1.75 million was estimated for the freshwater of the USA alone (Dodds et al., 2009). One of the causes of excess PO_4 in water is the lack of adequate PO_4 treatment and monitoring in waste water treatment plants (WWTP), in particular in ecologically more sensitive rural areas. For economic reasons classical waste water treatments that needs costly infrastructure are often not performed, *e.g.* installations using the activated sludge process in either low population, remote or developing areas. Therefore, WWTP using passive water treatment technologies such as reed bed filters are often preferred. Natural materials such as hydroxyapatite, or industrial waste such as steel slag, were used at the pilot scale to remove phosphate from wastewater (Vohla et al., 2011). If such materials are intended to be used in horizontal filters, the dimensioning of the reactors depends on numerous factors such as: (i) the number of population equivalent (PE) releasing wastewater, (ii) the quantity of P-PO_4 released by 1 PE per day {typically in the range of ~ 1 to ~3 g P-PO_4 PE^{-1} (Henze and Comeau, 2008)}, (iii) the PO_4 removal capacity (mg P-PO_4 g^{-1}) of the Filtration Material (FM) under hydrodynamic flow and (iv) the duration of the water treatment until the

material is saturated with PO_4. As an example, a volume of ~ 0.8 m^3 of FM per PE was estimated to be necessary for a 4 years treatment if ferrihydrite coated pozzolana was used as a FM (Ruby et al., 2016). Such a volume of FM corresponds also to a surface ~ 2 m^2 per PE for a horizontal filter with a depth of 0.5 m. Therefore, passive water treatments are generally extensive and need relatively high amount of FM that occupy a relatively large surface. As explained by Vohla (Vohla et al., 2011), large-scale and long-term (typically 5 years) experiments are absolutely necessary for evaluating accurately the optimal quantity and lifetime of the FM in such filters. A possibility for reducing the size of the filtration reactors is to synthesize FM characterized by a much higher PO_4 removal capacity. For this purpose, Layered Double Hydroxides (LDH) are particularly interesting materials. They constitute of stacking of hydroxide layers containing divalent M^{II} and trivalent M^{III} cations. The positive charge of the cationic sheets is counterbalanced by the presence of anions A^{n-} and water molecules present in the interlayer. LDH obey the general chemical formula $[M^{II}_{(1-x)}M^{III}_x(OH)_2]^{x+}$ $[x/n\ A^{n-}\ m\ H_2O]^{x-}$ where x represents both the charge of the layers and the M^{III} molar fraction. The values of x depend on the nature of the M^{II} and M^{III} cations and vary in a range from ~ 0.1 to 0.33 (Forano et al., 2013). LDH can remove PO_4 by several mechanisms such as adsorption, anionic exchange or dissolution-precipitation (Baliarsingh et al., 2013). The Theoretical PO_4 Removal Capacity of an LDH (TPRC in mg g^{-1}) by anionic exchange depends on the M^{III} molar fraction (x), the charge (n) of the replacing anions and on the LDH molar mass. As discussed later in this work, the maximal TPRC of Ca-Fe LDH will be estimated to be as high as ~ 110 mg P-PO_4 g^{-1}, a value much higher than the removal capacity reported in homogeneous batch dispersion for other minerals such as ferrihydrite {~ 26 mg P-PO_4 g^{-1} (Ruby et al., 2016)}, steel slag (up to ~ 2.4 mg PO_4 g^{-1} (Barca et al., 2012) or hydroxyapatite (0.3 mg P-PO_4 g^{-1} (Bellier et al., 2006)). Maximal phosphate removal capacities {$q_e^{(Max)}$} of the same order of magnitude than the TPRC were in fact reported by different authors studying the interaction of Ca based LDH such as Ca-Al LDH (Bekele et al., 2019; Jia et al., 2016; Oladoja et al., 2014; Qian et al., 2012), *i.e.* hydrocalumite, Ca-Mg-Al LDH (Ashekuzzaman et al., 2014) and Ca-Fe LDH (Ashekuzzaman et al., 2014; Tsuji and Fujii, 2014). However, for both Ca-Al LDH and Ca-Fe LDH, the reported values of

$q_e^{(Max)}$ varied in a relatively broad range between ~ 46 and ~ 179 mg P-PO_4 g^{-1} depending on experimental conditions, *e.g.* LDH synthesis procedure, phosphate concentration, adsorbent dose and pH. Several authors reported the mineralogical transformation of the LDH into a calcium phosphate phase such as hydroxyapatite (Qian et al., 2012; Tsuji and Fujii, 2014) or brushite (Bekele et al., 2019; Jia et al., 2016), in particular for high PO_4 concentrations (150 mg L^{-1} ≤ [PO_4] ≤ 1500 mg L^{-1}). At lower PO_4 concentrations, a significant decrease of intensity and a general broadening of the LDH X-ray diffraction (XRD) peaks were observed (Ashekuzzaman et al., 2014; Oladoja et al., 2014). The synthesis of Ca-Fe LDH was reported to lead to a higher degree of crystallinity in comparison to Mg-Al LDH, i.e. hydrotalcite (Tsuji and Fujii, 2014). However, the concomitant formation of secondary phases supposed to be $Ca(OH)_2$, "$Fe(OH)_3$" and $CaCO_3$ was noted when varying the Ca : Fe ratio between 0.75 and 3. In a recent study we demonstrated that almost single phase Ca-Fe LDH can only be synthesized for a Ca : Fe ratio of 2 : 1, with a higher ratio leading to the formation of either $Ca(OH)_2$ or $CaCO_3$ depending on the synthesis procedure (Al-Jaberi et al., 2015).

The first goal of this study was to determine as precisely as possible the mineralogical transformation of single phase Ca-Fe LDH in the presence of PO_4 solutions of varying concentrations. The behavior observed at lower PO_4 concentration (< ~ 100 mg L^{-1}) will be particularly relevant for application in waste water treatment where the concentration of PO_4 is often between ~ 10 and ~ 60 mg L^{-1} (Ruby et al., 2016). Moreover, we recently developed a new method of synthesis allowing the deposition of a high amount of ferrihydrite onto a pozzolana support (Ruby et al., 2015). Such a method of synthesis was adapted here to synthesize pozzolana coated with Ca-Fe LDH (Ca-Fe LDH-Pz). The second goal of this study was to study the PO_4 removal by Ca-Fe LDH-Pz under hydrodynamic conditions. Such an experiment is of upmost importance if the material is finally intended to be used for horizontal, or vertical, filters in the field.

2. Experimental

2.1 Chemical Products

Calcium chloride dihydrate ($CaCl_2.2H_2O$), iron (III) chloride hexahydrate ($FeCl_3.6H_2O$) and sodium hydrogenophosphate dehydrate ($NaH_2PO_4.2H_2O$) were purchased from Sigma-Aldrich with a purity greater than 99%. Sodium hydroxide was procured from Carlo Erba with purity greater than 99%. The pozzolana (Pz) was supplied by "Pouzzolanes des Domes" (Saint-Ours-les-Roches, France) and was characterized by a grain size ranging from 1 to 3 mm. As already described previously (Ruby et al., 2015), pozzolana is a porous material comprised of a mixture of labradorite (Na,Ca) $(Al,Si)_4O_8$, diopside $CaMgSi_2O_6$, forsterite Mg_2SiO_4 and hematite α-Fe_2O_3.

2.2 Materials synthesis

2.2.1 Synthesis of Ca-Fe LDH

The method of synthesis of the Ca-Fe LDH was optimized in a previous study (Al-Jaberi et al., 2015). Briefly, a first solution (A) was prepared by dissolving 66.7 mmol of Ca(II) and 33.3 mmol of Fe(III) salts (Ca(II) : Fe(III) = 2 : 1) into 300 mL of demineralized ultrapure water (18.2 MΩ). Solution A was introduced progressively with the help of a peristaltic pump (total time of 150 min.) into a 300 mL solution B containing 200 mmol of NaOH (OH^- / {Ca(II) + Fe(II)} = 2) to precipitate the LDH product. At the end of the experiment the pH was between 11.4 and 11.8. The LDH dispersion was filtered under suction through a Buchner funnel using 22 μm pore size Millipore© paper filter. All the filtered samples were thoroughly washed with distilled water and cold ethanol, dried at room temperature and ground in a mortar to obtain a fine powder.

2.2.2 Synthesis of Ca-Fe LDH coated pozzolana

A mass of 20 g of Ca-Fe powder was mixed with 100 g of Pz in a dry state in a 500 mL plastic wide necked bottle. The mixture was shaken during 12 h using a Reax 20/8 overhead shaker (Heidolph Intruments GmbH& Co.K.G, Schwabach, Germany) with a rotation speed of 16 rpm. The LDH coated Pz was subjected to the separation of free particles with a 40 mesh sieve. The quantity of LDH

deposited onto Pz was estimated to be 14.2 $\pm$ 0.4 g% by comparing the weight of the material before and after coating.

2.3 Characterization of the samples

2.3.1 X-Ray Diffraction (XRD).

The crystal structure of the samples was studied by XRD using a Philips X'Pert pro MPD diffractometer (CuKα radiation λ = 1.5418 Å). Patterns were collected with a step size of 0.03342 ° and a rate of 87.63 s per step.

2.3.2 Raman spectroscopy

Raman spectra were recorded in backscattering configuration by using a Horiba Jobin-Yvon T64000 spectrometer, equipped with an Ar^{2+} laser emitting at 514.53 nm in the range 100 to 4000 cm^{-1}. The spectrum was setup with a 1800 groove mm^{-1} diffraction grating, and a liquid N_2-cooled Charge Coupled Device (CCD). The spectra resolution was set to 2 cm^{-1} by selecting the entrance slit width. The objective was x80 (0.95 of numerical aperture). The spectrometer was calibrated with the 520.7 cm^{-1} line of a silicon wafer. The laser power was 200 mW.

2.3.3 Mössbauer spectrometry

Transmission Mössbauer spectrometry was performed using a ^{57}Co source to identify the iron containing compounds. The filtered materials were transferred inside a cold head cryostat (Advanced Research Systems) under an inert He atmosphere. Mössbauer spectra were recorded with a constant acceleration spectrometer and a 512 multichannel analyser. The data were calibrated with a 25 µm thick pure α-iron foil. Mössbauer spectra were fitted using the Recoil software. Shape lines were either Lorentzian or Voigt profile, *i.e.* a convolution of a Gaussian distribution with a Lorentzian shape line.

2.3.4 Transmission Electron Microscopy (TEM).

The data were collected at the Competence Center for Electronics Microscopy and Microwaves (Institut Jean Lamour UMR 7198 CNRS-Université de Lorraine) by using a JEOL JEM-ARM200F

apparatus. The sample was prepared by forming a dispersion of the dried solid product into ethanol. One drop of the dispersion was laid on a copper grid for TEM analysis coupled with an Energy Dispersive X-ray (EDX) analyzer.

2.3.5 X-Ray Photoelectron spectroscopy (XPS)

XPS spectra were recorded by using a Kratos Axis Ultra DLD (Manchester, UK) instrument. The spectra were recorded at a normal (90°) angle between the surface of the sample and the direction of the ejected electron. The acquisition of low-resolution spectra has been carried out with pass energy of 160 eV and steps of 1 eV and high resolution spectra with a pass energy of 20 eV and steps of 0.5 eV. The analyzed area was 0.3x0.7 mm^2. The spectra were corrected for charging effects by using the C1s contamination peak situated at 284.6 eV.

2.3.6 Inductive Coupled Plasma Atomic Emission Spectroscopy (ICP-AES)

Dissolved phosphate, calcium and iron species concentrations were measured by ICP-AES using a Jobin Yvon-ULTIMA apparatus. The solutions were mixed into HNO_3 solutions to avoid the presence of trace solid particles before analysis.

2.4 Chemical reactivity of Ca-Fe LDH with phosphate

2.4.1 Batch experiments

Phosphate solutions with various concentrations were prepared by dissolving $NaH_2PO_4.2H_20$ into ultrapure water. All experiments were conducted at room temperature with a 0.1 M NaCl supporting electrolyte and a pH of 7. All the pH measurements were carried out with a digital pH meter (Almemo model 2690) using a glass electrode (model PHER 112 SE). The pH of the solutions was adjusted manually to the required values by diluted NaOH or HCl solutions. The volume of acid/alkali added for pH adjustment never exceeded 1% of the total volume. The PO_4 removal kinetics was studied over 48 h by adding 1 g of LDH in 1 L of phosphate solution, with concentrations varying in between 20 and 1000 mg L^{-1} (0.21 to 10.53 mmol L^{-1}). The effect of the initial PO_4 concentrations (isotherm experiments) was studied in another set of experiments where 0.1 g of LDH was

175 introduced into 100 mL of PO_4 solution with an initial concentration varying between 20 and 2000 mg
176 L^{-1} for 24 h, this time period having been previously determined from kinetics experiments as being
177 sufficient for reaching quasi-equilibrium conditions. At a selected time, 1 mL of the solution was
178 withdrawn to determine PO_4 concentrations by ICP-AES and, as required, also other soluble species
179 such as Ca^{2+}_{aq} and Fe^{3+}_{aq}. Each run was performed in duplicate and the results were averages of the
180 two trials with reproducibility within $\pm$ 5%.
181 *2.4.2 Column flow through experiments*
182 The column experiment was conducted in a Plexiglas© column with 3.7 cm internal diameter and 50
183 cm height. The column was loaded with 482 g of LDH coated Pz. The feed solution
184 ([PO_4] = 100 mg L^{-1}) was continuously pumped in an up-flow mode from the reservoir through the
185 column at a flow rate of 1.1 mL min^{-1} using a peristaltic pump. The contact time was ~ 5.5 h. Samples
186 were taken at regular time intervals in the outflow (2 sample per day) for 70 days for performing
187 chemical analyses with ICP-AES.
188
189 **3. Results**
190 3.1 Dissolution properties of Ca-Fe LDH in pure water
191 *3.1.1 Measurement of soluble Ca and Fe species*
192 Dried Ca-Fe LDH was introduced into demineralized water ([LDH] = 1 g L^{-1}) under continuous stirring.
193 While soluble Fe concentration stayed below the detection limit of the ICP-AES due to the very low
194 solubility of Fe(III) species in alkaline solution, the soluble Ca concentration exhibited a strong
195 increase during the first 4 hours and reached a threshold value of 203 mg L^{-1} (Fig. 1). This value was in
196 line with the concentration of Ca measured in the solids of the pristine Ca-Fe LDH (300.5 mg g^{-1}) and
197 the hydrolysed product (100.6 mg g^{-1}). Therefore about 2/3 of the Ca species initially present in the
198 solid was released into solution and 1/3 was in a solid state. After a contact time of 48 hours the final
199 pH of water was 11.8.
200

3.1.2 Mineralogical transformation of Ca-Fe LDH in pure water.

The XRD patterns of the pristine LDH exhibited hydrocalumite-like structure (PDF 44-0445) (Fig. 2 a). The pattern was indexed in a hexagonal lattice with a R-3 rhombohedral space group symmetry. A d003-value of 7.77 Å was calculated in very good agreement with the value of 7.72 Å reported for Ca-Fe-Cl LDH (Tsuji and Fujii, 2014). After a contact time with water of 24 h, the Ca-Fe LDH was completely transformed as testified by the absence of LDH diffraction lines (Fig 2b). The resultant diffraction lines were attributed to the formation of $CaCO_3$ meaning that a part of the Ca species present initially into the LDH reacted with carbonate ions present in water under the strong alkaline conditions. Raman spectroscopy was used to identify the solid phase containing the Fe^{III} species. Very similar features to those recorded previously for two-line ferrihydrite were observed by Raman spectroscopy (Fig. 2c&d). Indeed, the main bands of the ferrihydrite Raman spectra were reported to be situated at 223, 288 and 390 cm^{-1} (Root et al., 2012). Two-line ferrihydrite also generally exhibited 2 low intensity XRD diffraction peaks that were not clearly observed here (Fig. 2b), most probably due to the formation a very disordered ferric structure in comparison to the well crystallised $CaCO_3$ compound. The full dissolution of the Ca-Fe LDH was confirmed by XPS, and, indeed, the chloride ions intercalated in the LDH were not detected with XPS anymore after 24 hours of contact time in water (Fig. SI-1).

3.2 Reactivity of Ca-Fe LDH with phosphate

3.2.1 Phosphate removal in batch experiments

The quantity of phosphate (PO_4) removed from water, q (mg P-PO_4 g^{-1}), was recorded (Fig. 3a) during a period of 48 hours for a series of initial PO_4 concentrations ranging from 25 mg L^{-1} to 1000 mg L^{-1} ([LDH] = 1 g L^{-1}). The quantity of PO_4 removed from water increased rapidly during the first 4 hours and reached a maximum value in between less than ~1 hour and ~ 8 hours for increasing PO_4 concentrations. As expected, the maximum value was achieved more quickly at low PO_4 concentrations. The maximum PO_4 removal obtained after 48 hours of contact time was plotted as a

function of the initial PO_4 concentrations (Fig 3b). The linear increase recorded in Zone A of the curve corresponds to experiments where the removal rate *R* was equal or very close, to 100%. In this case the concentration of PO_4 removed from the water was simply equal to the quantity of PO_4 introduced into the solution. A maximum removal capacity, q_{Max} , of the Ca-Fe LDH is measured at higher PO_4 concentrations in zone B where *R* is lower than 100%. The value q_{Max} is close to 130 mg P-PO_4 g^{-1} for the highest initial PO_4 concentration of 1000 mg L^{-1} and is relatively high in comparison to those reported for Ca-Fe LDH, *i.e.* in between ~ 46 and ~ 91 mg P-PO_4 g^{-1} (Table 1). The value of q_{Max} is also significantly higher than the adsorption capacity of ferrihydrite (~ 20 mg PO_4 g^{-1} < q_{Max} < ~ 33 mgP-PO_4 g^{-1} in the pH range between 9 and 4, respectively). Note that ferrihydrite with a Surface Specific Area (SSA) of ~ 300 m^2 g^{-1} was reported to be the best PO_4 adsorbent of the iron oxide mineral family (Ruby et al., 2016). This comparison with ferrihydrite suggests that Ca-Fe LDH interacted with PO_4 *via* another mechanism than a simple adsorption process allowing the removal of a much higher quantity of PO_4.

3.2.2 Mineralogical transformation of LDH in contact with PO_4

The solid products obtained after 48 hours of contact of the LDH with various PO_4 solutions were analysed with XRD (Fig. 4). At a low PO_4 concentration (Fig. 4b), the XRD pattern obtained was quite similar to the one observed previously in PO_4-free water (Fig. 2b) and exhibited only the peaks of $CaCO_3$. For increasing PO_4 concentrations, new broad diffraction peaks appeared and sharpened progressively at higher PO_4 concentrations (Fig 4c). These new peaks were attributed to the formation of hydroxyapatite (HA) {$Ca_5(PO_4)_3OH$, PDF 41-0490}. The progressive disappearance of the $CaCO_3$ XRD peaks was concomitant with the progressive appearance of the HA XRD peaks (Fig. 4b-d). The kinetics of transformation of the LDH as function of time was also studied for an initial PO_4 concentration of 600 mg L^{-1} (Fig. 5). In the very initial stages of the reaction, *e.g.* 10 min of reaction (Fig. 5b), the intensity of the LDH peaks decreased and traces of $CaCO_3$ and HA were detected. The disappearance of the diffraction peaks attributed to $CaCO_3$ and LDH occurred after 30 min and 4 h of

reaction times, respectively. Therefore, both $CaCO_3$ and the LDH were dissolved into soluble Ca^{2+}_{aq} species that partially precipitated with PO_4 to form HA. The dissolution of the LDH was much faster (30 min) in the presence of a lower PO_4 concentration of (20 mg L^{-1}) and the final solid product was in this case $CaCO_3$ (Fig. SI2).

3.2.3 Correlation between the concentrations of soluble Ca and PO_4 species

The evolution of the PO_4 and Ca in solution after 48 h. of interaction between the LDH and PO_4 was plotted as a function of the initial phosphate concentration (Fig. 6). In order to perform a mass balance for the reactions, the concentrations were reported in mmol L^{-1} (1 mmol L^{-1} of PO_4 corresponds approximatively to 100 mg L^{-1} of PO_4). The soluble calcium concentration decreased almost linearly in zone A (0.2 mmol L^{-1} ≤ $[PO_4]_0$ ≤ 2 mmol L^{-1}) when PO_4 anions were completely removed by the LDH. For a critical PO_4 concentration of ~ 2 mmol L^{-1}, the Ca^{2+}_{aq} concentrations reached a value close to zero and the PO_4 concentration began to increase. For $[PO_4]_0$ values higher than ~ 2 mmol L^{-1}, the PO_4 concentration increased linearly with a slope of 1, meaning that an excess of PO_4 remained fully in solution. The slope of the linear decrease of PO_4 concentration [0.2 mmol L^{-1} - 2 mmol L^{-1}] was measured to be close to 5 : 2 (Ca : PO_4 = 2.5), a value significantly higher than the one expected if one considers that phosphate was only removed by the precipitation of hydroxyapatite $Ca_5(PO_4)_3OH$ (Ca : PO_4 = 1.67). This result suggests that PO_4 was removed from water by another mechanism, or a combination of mechanisms.

3.2.4 Complementary analysis of the solid products obtained at low phosphate concentrations

The XRD patterns obtained after the interaction of the LDH with PO_4 at low concentration did not clearly exhibit the diffraction pattern of HA (Fig. 4 b-c), and therefore further investigations were performed with TEM and Mössbauer spectroscopy. The products of transformation of the LDH with $[PO_4]_0$ = 20 mg L^{-1} consisted of $CaCO_3$ crystals mixed with an agglomeration of nanocrystals (Fig. 7). Chemical analysis with EDX of the nanocrystals revealed the presence of O, Fe, Ca and P atoms

276 (Table 2). P atoms were not detected on $CaCO_3$ crystals (spot C & F) showing that calcite was inactive
277 for PO_4 removal. The chemical composition of the agglomerated nanocrystal was relatively
278 heterogeneous: calcium rich zones were detected in some areas (spots A, B, D & G) while iron rich
279 zones were detected in other areas (spots H & E). These nanocrystals containing Fe^{III} species were
280 assigned to the presence of a ferric paramagnetic doublet when probed with Mössbauer
281 spectroscopy at 77 K (Fig. 8a). The magnetic transition occurred at a temperature situated around 35
282 K (Fig. 8b) and the Mössbauer spectra recorded at 14 K was essentially constituted of a distribution
283 of very broad sextets. A broad ferric doublet D_1 (RA of 10%) was added to obtained a good fit of the
284 central part of the spectrum (Table 3). The very broad range of the hyperfine field measured for the
285 sextet's distribution was situated in between 133 and 453 kOe such as those arising from
286 superparamagnetism. This observation was in agreement with the TEM data previously shown (Fig.
287 7), corresponding to the formation of chemically heterogeneous nanocrystals containing Fe(III) and
288 Ca(II) species.

289 *3.2.5 Column flow through experiments*

290 The potential of Ca-Fe LDH coated pozzolana for removing PO_4 was evaluated under hydrodynamic
291 conditions. The quantity of PO_4 measured in the outflow of the column ($[PO_4] / [PO_4]_0$) and the pH
292 were recorded as a function of V / V_p (Fig 9), where $[PO_4]_0$ is the concentration of phosphate in the
293 inflow = (100 mg L^{-1}), V is the total volume occupied by the filtration material and V_p the porous
294 volume. The pH in the outflow increased very rapidly from 4.6 to 11.3, in agreement with the LDH
295 dissolution process observed previously in homogeneous batch experiments. In the first step, the pH
296 decreased only very slowly and, in a second step, a sharp decrease was observed after 43 days of
297 experiments corresponding to a V / V_p value of 188. This value was also the critical volume
298 corresponding to the breakthrough of the column by the phosphate species: a sharp increase of the
299 $[PO_4] / [PO_4]_0$ value was observed and the concentration of PO_4 in the outflow was almost identical to
300 the concentration of PO_4 in the inflow ($[PO_4] / [PO_4]_0 \sim 1$) after 70 days of experiment.

4. Discussion

4.1. Reactivity of Ca-Fe LDH with phosphate in batch experiments

4.1.1 Removal capacity at high phosphate concentration (> 100 mg L^{-1})

Three types of reactions were considered in order to evaluate the corresponding phosphate removal capacity. LDH are well known to be anion exchange materials and the question whether such a process could be responsible for a phosphate removal capacity as high as ~ 400 mg L^{-1} arises. The removal capacity by anionic exchange is strongly dependent on the speciation of the phosphate species (PO_4^{3-}, HPO_4^{2-} or $H_2PO_4^-$) present in the interlayer. Let us consider the intercalation of a monovalent $H_2PO_4^-$ that should lead to the maximal removal capacity *via* anionic exchange corresponding to the following chemical reaction:

$$\{[Ca^{II}_4Fe^{III}_2(OH)_{12}]^{2+} \bullet 2Cl^-\} + 2\ H_2PO_4^- = \{[Ca^{II}_4Fe^{III}_2(OH)_{12}]^{2+} \bullet 2H_2PO_4^-\} + 2Cl^- \quad (1)$$

This reaction leads to a maximal removal capacity by anionic exchange of 113 mg P-PO_4 g^{-1} slightly lower than the value measured in this study. According to the solid analysis, hydroxyapatite (HA) and a ferric (hydr)oxide are the main products of transformation of the LDH. This corresponds to the following chemical reaction:

$$5\ \{[Ca^{II}_4Fe^{III}_2(OH)_{12}]^{2+} \bullet 2\ Cl^-\} + 12\ H_2PO_4^- = 4\ Ca_5(PO_4)_3(OH) + 10\ FeOOH + 2\ OH^- + 10\ Cl^- + 34\ H_2O \quad (2)$$

This reaction leads to a removal capacity by dissolution-precipitation of 135 mg P-PO_4 g^{-1}, which is in better agreement with the value measured in this study. Note that the formation of a {HA, $FePO_4$} mixture would have led to an even higher removal capacity, of around 244 mg P-PO_4 g^{-1}. Considering reaction (2), one may hypothesize that at high phosphate concentration the removal of PO_4 was essentially governed by the dissolution of Ca^{II} species present in the initial LDH reactant. A part of the phosphate species may also be adsorbed on the ferric (hydr)oxide nanocrystals but the relative proportion of this process in the overall phosphate removal was certainly lower. Indeed the PO_4

removal capacity of ferric (hydr)oxides is generally situated in a significantly lower range between 3 and 26 mg P-PO_4 g^{-1} (Mallet et al., 2013).

4.1.2 Removal capacity at low phosphate concentration (≤ 100 mg L^{-1})

The XRD patterns showed the progressive disappearance of HA when the phosphate concentration decreased (Fig 5). This decrease was concomitant with a progressive decrease of the PO_4 removal capacity. In the concentration range 25 - 100 mg L^{-1}, calcite $CaCO_3$ is formed rather than HA. Therefore, a competitive association of Ca either with phosphate or carbonate was evidenced. This competition was won either by phosphate, or by carbonate, at high and low PO_4 concentration, respectively.

TEM showed that calcite ($CaCO_3$) did not adsorb PO_4 species that were rather associated with a very disordered solid phase containing both Ca^{II} and Fe^{III} species. Therefore, a significant proportion of the Ca^{II} species initially present in the LDH phase did not participate to the PO_4 removal and are either released as soluble species or present in $CaCO_3$. However, a minor part of the Ca species coexists with Fe species in a solid phase resembling ferrihydrite. As previously described (Ruby et al., 2016) the co-existence of Ca species and ferrihydrite led to a global increase of PO_4 removal in comparison to Ca free ferrihydrite. Such a synergistic effect may explain the relatively high PO_4 removal observed even at low PO_4 concentrations in this study, e.g. for an initial PO_4 concentration of 100 mg L^{-1}, the removal capacity was not determined accurately since the removal rate was close to 100% and the Fe-Ca solid surfaces are certainly under-saturated. However, the data showed that the removal capacity is at least as high as 33 mg P-PO_4 g^{-1}, a value higher than those measured for Ca free iron oxides (Ruby et al., 2016).

4.2 Reactivity of Ca-Fe LDH with phosphate in column experiment

The experiment performed in the column demonstrated that pozzolana (Pz) coated with Ca-Fe LDH was particularly efficient for removing phosphate. Indeed, the experiment may be compared to

348 another set of column experiments performed recently using ferrihydrite (Fh) coated Pz (Ruby et al.,
349 2015; Ruby et al., 2016) where the experimental conditions were quite similar, *i.e.* identical
350 dimensions of the columns, [PO_4]= 100 mg L^{-1} in the inflow, but with a contact time of ~ 8 h instead
351 of ~ 5.5 h in this study. The removal capacity measured here at the breakthrough for Ca-Fe LDH-Pz,
352 *i.e.* q_B ~ 4 mg P-PO_4 g^{-1}, was ~ 3.2 times higher than the value measured previously for Fh-Pz, *i.e.* q_B ~
353 1.3 mg P-PO_4 g^{-1}. However, the pH values higher than 11 measured in the outflow represent a
354 problem for an eventual application for waste water treatment. Indeed, such pH values are
355 significantly higher than the usual discharge standards with pH values that should be situated in
356 between 6 and 8.5. In order to use Ca based LDH materials for such an application, a better control of
357 the LDH dissolution properties would be necessary. On one hand the dissolution of Ca is beneficial
358 for PO_4 removal by precipitation, but on the other hand the LDH dissolution leads also to the release
359 of OH^- species by inducing an increase of pH {see equation (2)}. According to the different reactions
360 paths obtained in batch experiments (Fig. 10), a significant proportion of the Ca species present in
361 the LDH was not efficient for PO_4 removal and was released in the aqueous medium. A decrease of
362 the solubility of the LDH may be obtained by introducing in the solid structure less soluble divalent
363 species than Ca^{2+} such as Mg^{2+} (Ashekuzzaman et al., 2014). Tuning carefully the relative proportion
364 of Ca^{II} and Mg^{II} in a ternary Ca^{II}-Mg^{II}-Fe^{III} LDH system in order to control both the resulting pH at
365 lower values and the amount of dissolved Ca^{2+} and Mg^{2+} could be an interesting way to enhance the
366 applicability of using these LDH materials for PO_4 removal in wastewater. Less soluble LDH such as
367 Mg-Al hydrotalcite or Mg-Fe pyroaurite may also remove PO_4 by anionic exchange, a process that can
368 be concomitant to adsorption or precipitation of phosphate species. Natural hydroxyapatite or shell-
369 sand was also studied for removing PO_4 from wastewater; similarly a slow release of Ca^{2+} soluble
370 species was suggested as an efficient way for driving PO_4 removal by a surface precipitation process
371 (Lyngsie et al., 2014; Molle et al., 2005).

372

5. Conclusion

The interaction between Ca-Fe layered double hydroxide and phosphate species was studied both in homogeneous dispersion and in a flow through column experiment. In phosphate free water, the LDH was fully transformed into a mixture of a ferrihydrite-like Fe^{III}-Ca^{II} disordered solid phase, calcite $CaCO_3$ and soluble Ca^{2+}_{aq} species. At high phosphate concentration ($[PO_4] > 100$ mg L^{-1}), Ca^{2+}_{aq} species released by the LDH precipitated as hydroxyapatite leading to the removal of a very high concentration of phosphate ($q_e \sim 130$ mg P-PO_4 g^{-1}). At low phosphate concentration ($[PO_4] \leq 100$ mg L^{-1}), phosphate is most probably removed by adsorption on the ferrihydrite-like Fe^{III}-Ca^{II} compound. Pozzolana coated with Ca-Fe LDH very efficiently removed phosphate from water under hydrodynamic conditions, the breakthrough of the column occurring at least 3 times later in comparison to ferrihydrite coated pozzolana (Ruby et al., 2015). However, the high solubility of the Ca-Fe LDH led also to a strong increase of the pH (> 11) preventing any direct application of such a material for wastewater treatment. Future work dedicated to the control of the slow release of Ca^{2+}_{aq} and OH^- species leading to a partial dissolution of the LDH may improve the overall performance of the material, *i.e.* a high PO_4 removal capacity and concomitantly limited alkaline modification of the aqueous medium.

Acknowledgment

We would like to thank the Ministry of Higher Education and Scientific Research of Irak for the PhD grant of Muayad Al-Jaberi. The authors would like also to thank Ghouti Medjahdi (CNRS, Institut Jean Lamour, Université de Lorraine) for TEM experiments. Claire Genois and Manuel Dossot (LCPME, Institut Jean Barriol, Université de Lorraine) are acknowledged for their help during ICP-AES and Raman Spectroscopy experiments. Prof C. Ruby and Prof. C. Greenwell thank the Institute of Advanced Study of Durham University for the collaborative opportunity. Indeed, C. Ruby was an IAS invited fellow in Durham University from October to December 2017.

References

[1] Al-Jaberi, M., Naille, S., Dossot, M., Ruby, C., 2015. Interlayer interaction in Ca–Fe layered double hydroxides intercalated with nitrate and chloride species, J. Mol. Struct. 1102, 253-260.

[2] Ashekuzzaman, S. M., Jiang, J.-Q., 2014. Study on the sorption-desorption-regeneration performance of Ca-, Mg and CaMg-based layered double hydroxides for removing phosphate from water, Chem. Eng. J. 246, 97-105.

[3] Baliarsingh, N.; Parida, K. M.; Pradhan, G. C., 2013. Influence of the nature and concentration of precursor metal ions in the brucite layer of LDHs for phosphate adsorption - a review, RSC Adv. 3, 23865-23878.

[4] Barca, C., Gérente, C., Meyer, D., Chazarenc, F., Andrès, Y., 2012. Phosphate removal from synthetic and real wastewater using steel slags produced in Europe, Water Res. 46, 2376-2384.

[5] Bekele, B., Lundehøj, L., Jensen, N. D., Nielsen, U. G., Forano, C., 2019. Sequestration of orthophosphate by Ca_2Al-NO3 layered double hydroxide – Insight into reactivity and mechanism, Appl. Clay Sci. 176, 49-57.

[6] Bellier, N., Chazarenc, F., Comeau, Y., 2006. Phosphorus removal from wastewater by mineral apatite, Water Res. 40, 2376-2384.

[7] Dodds, W. K., Bouska, W. W., Eitzmann, J. L., Pilger, T. J. , Pitts, K. L., Riley, A. J., Schloesser, J. T. Thornbrugh, D. J., 2009. Eutrophication of U.S. Freshwaters: Analysis of Potential Economic Damages, Environ. Sci. Technol 43 , 12-19.

[8] Forano, C., Costantino, U., Prévot, V., TaviotGueho, C., 2013. Chapter 14.1 - Layered Double Hydroxides (LDH), Developments in Clay Science 5, 745-782.

[9] M. Henze, Y. Comeau, 2008. Wastewater characterization in M. Hence, M.C.M. van Loosdrecht, G.A. Ekama, D. Brdjanovic (Eds.), Biological Wastewater Treatment: Principles, Design and Modelling, IWA Publishing, London, pp 33-52.

[10] Jia, Y., Wang, H., Zhao, X., Liu, X., Wang, Y., Fan, Q., Zhou, J., 2016. Kinetics, isotherms and multiple mechanisms of the removal for phosphate by Cl-hydrocalumite, Appl. Clay Sci. 129, 116-121.

[11] Lyngsie, G., Borggaard, O.K., Hansen, H. C. B., 2014. A three-step test of phosphate sorption efficiency of potential agricultural drainage filter materials, Water Res. 51, 256-265.

[12] Mallet, M., Barthélémy, K.,Ruby, C., Renard, A., Naille, S., 2013. Investigation of phosphate adsorption onto ferrihydrite by X-ray Photoelectron Spectroscopy, J. Colloid Interface Sci. 407, 95-101.

[13] Molle , P., Liénard, A. ,Grasmick, A., Iwema A., Kabbabi, A. 2005. Apatite as an interesting seed to remove phosphorus from wastewater in constructed wetlands, Water Sci. Technol. 51, 193-203.

[14] Oladoja , N.A., Adelagun, R.O.A., Ololade, I.A., Anthony, E.T., Alfred, M.O., 2014. Synthesis of nano-sized hydrocalumite from a Gastropod shell for aquasystem phosphate removal, Sep. Purif. Techol. 124, 186-194.

[15] Qian, G., Feng, L., Zhou, J. Z., Xu, Y., Liu, J., Zhang, J., Xu, Z. P., 2012. Solubility product (Ksp)-controlled removal of chromate and phosphate by hydrocalumite, Chem. Eng. J., 181-182, 251-258.

[16] Rietra, R. P. J. J., Hiemstra, T., van Riemsdijk, W. H., 2001. Interaction between calcium and phosphate adsorption on goethite, Environ. Sci. Technol., 35, 3369-3374.

[17] Rout, K., Mohapatra, M., Anand, S., 2012. 2-Line ferrihydrite: synthesis, characterization and its adsorption behavior for removal of Pb(II), Cd(II), Cu(II) and Zn(II) from aqueous solutions, Dalton Trans. 41, 3302-3312.

441 [18] Ruby, C., Barthélémy, K., Hanna, K., Mallet, M., Naille, S., 2015. Synthesis process and
442 hydrodynamic behavior of a new filtration material for passive wastewater dephosphatation, Mater.
443 Des. 86, 168-177.

444 [19] Ruby, C., Naille, S., Ona-Nguema, G., Morin, G., Mallet, M., Guerbois, D., Barthélémy, K., Etique,
445 M., Zegeye, A., Zhang, Y., Boumaïza, H., Al-Jaberi, M., Renard, A., Noël, V., Binda, P., Hanna, K.,
446 Despas, C., Abdelmoula, M., Kukkadapu, R., Sarrias, J., Albignac, M., Rocklin, P., Nauleau, F., Hyvrard
447 N., Génin, J.-M., 2016. Use of Ferrihydrite-Coated Pozzolana and Biogenic Green Rust to Purify Waste
448 Water Containing Phosphate and Nitrate, Curr. Inorg. Chem 6, 100-118.

449 [20] Tsuji, H., Fujii, S., 2014. Phosphate recovery by generating hydroxyapatite via reaction of calcium
450 eluted from layered double hydroxides, Appl. Clay Sci. 99, 261-265.
451 [21] Vohla, C., Kõiv, M., Bavor, H. J., Chazarenc, F., Mander, Ü., 2011. Filter materials for phosphorus
452 removal from wastewater in treatment wetlands—A review, Ecol. Eng. 37, 70-89.

453

Figure captions

Figure 1: Evolution of soluble Ca^{2+} and Fe^{3+} concentrations in the supernatant during the interaction of Ca-Fe LDH with P-free demineralized water.

Figure 2: Evolution of the XRD patterns (a and b) and Raman spectra (c and d) during the interaction of Ca-Fe LDH with P-free demineralized water. (a) and (c) Pristine Ca-Fe LDH materials; (b) and (d) after contact with P-free demineralised water during 24 hours.

Figure 3: (a) Evolution the PO_4 removal capacity of Ca-Fe LDH as a function of time for different initial phosphate concentrations. (b) Evolution of the maximal removal capacity as a function of the initial phosphate concentration.

Figure 4: (a) Evolution the XRD patterns for Ca-Fe LDH after contact with PO_4 for different initial phosphate concentrations. (a) Pristine Ca-Fe LDH materials, (b) $[PO_4]_0$ = 20 mg L^{-1}, (c) $[PO_4]_0$ = 100 mg L^{-1}, (d) $[PO_4]_0$ = 200 mg L^{-1}, (e) $[PO_4]_0$ = 300 mg L^{-1}, (f) $[PO_4]_0$ = 400 mg L^{-1}, (g) $[PO_4]_0$ = 500 mg L^{-1}, (h) $[PO_4]_0$ = 600 mg L^{-1}.

Figure 5: (a) Evolution the XRD patterns for Ca-Fe LDH after contact with PO_4 solution ($[PO_4]_0$ = 600 mg L^{-1}) for different contact times.

Figure 6: Ions concentrations release from Ca-Fe LDH during the removal process at initial PO4 concentrations from 20 to 1000 mg L^{-1} (0.21 to 10.35 mmoL L^{-1}). The samples were taken after 48 hours of reaction.

Figure 7: TEM images of the transformation products obtained after the interaction of the Ca-Fe LDH with a PO_4 solution ($[PO_4]_0$ = 20 mg L^{-1}).

Figure 8: Mössbauer spectra of the transformation products obtained after the interaction of the Ca-Fe LDH with a PO_4 solution ($[PO_4]_0$ = 20 mg L^{-1}). The spectra were recorded at a temperature of 77 K (a), 35 K (b) and 14 K (c).

Figure 9: Evolution of the relative phosphate concentration C / C_0 as a function of V / Vp, where C represents the phosphate concentration in the outflow of the column, C_0 the phosphate concentration in the inflow of the column, V the volume of PO_4 solution introduced in the column and V_p the porous volume of the column. The evolution of the pH during this experiment is also represented.

Figure 10: Schematic description of the interaction of Ca-Fe LDH in interaction PO_{4aq} species as a function of the initial phosphate concentration: (a) $[PO_4]_0 \leq 100$ mg L^{-1} and (b) $[PO_4]_0 > 100$ mg L^{-1}. HA is hydroxyapatite.

Table captions

Table 1 : Maximal phosphate removal capacity measured by adsorption isotherms for various calcium containing LDH. If available, the values of the initial PO_4 concentration, the LDH dose and the pH of the isotherm experiments are also reported.

Table 2: Chemical analysis by EDX of the products of transformation of Ca-Fe LDH in contact with an initial PO_4 concentration of 20 mg L^{-1}. Three different regions of the sample were analysed.

Table 3 : Hyperfine parameters of the Mössbauer spectra (Fig. 8) measured after contact of a Ca-Fe LDH with a 20 mg L^{-1} phosphate solution.

Figure 1

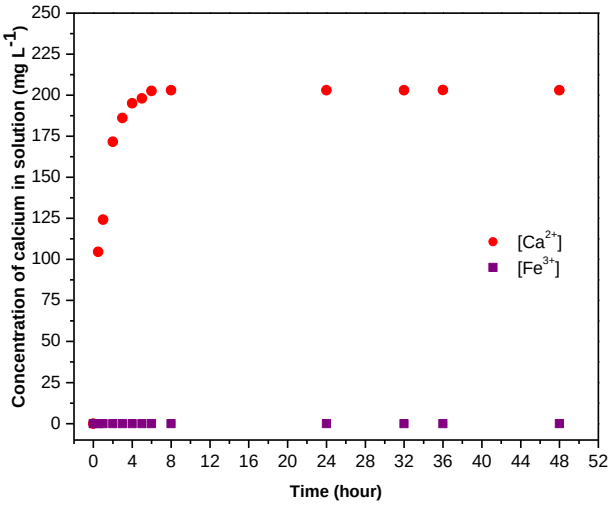
Concentration of calcium in solution (mg L-1)
250
225
200
175
150
125
100
75
50
25
0
0
4
8
12
16
20
24
28
32
36
40
44
48
52
Time (hour)
[Ca2+]
[Fe3+]

Figure 2

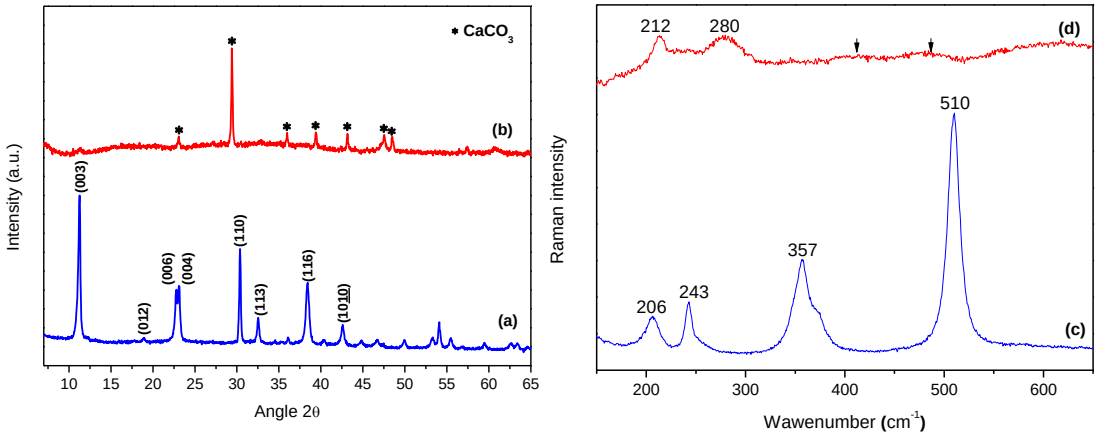
* CaCO3
(b)
(a)
(003)
(012)
(006)
(004)
(110)
(113)
(116)
(1010)
Intensity (a.u.)
Angle 2θ
10 15 20 25 30 35 40 45 50 55 60 65
212
280
(d)
510
357
206
243
(c)
Raman intensity
Wawenumber (cm-1)
200 300 400 500 600

Figure 3

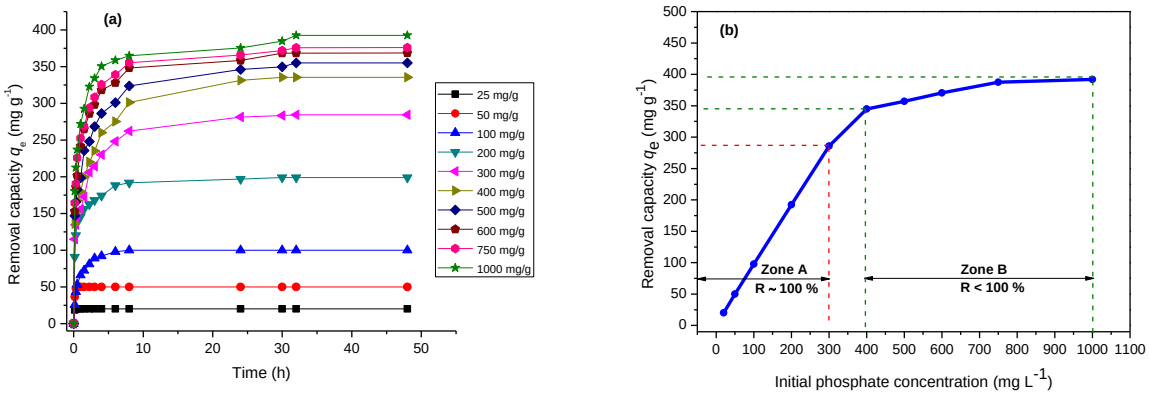
(a)
Removal capacity q_e (mg g^{-1})
Time (h)
25 mg/g
50 mg/g
100 mg/g
200 mg/g
300 mg/g
400 mg/g
500 mg/g
600 mg/g
750 mg/g
1000 mg/g
(b)
Removal capacity q_e (mg g^{-1})
Initial phosphate concentration (mg L^{-1})
Zone A
R ~ 100 %
Zone B
R < 100 %

Figure 4

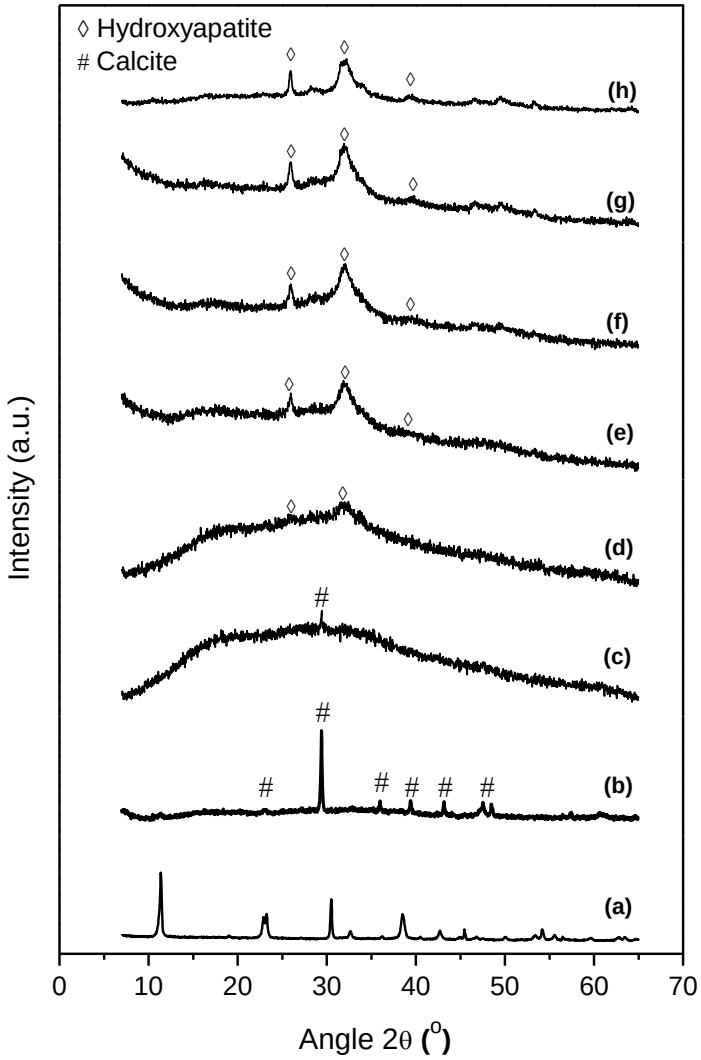
◊ Hydroxyapatite
Calcite
(h)
(g)
(f)
(e)
(d)
(c)
(b)
(a)
Intensity (a.u.)
0
10
20
30
40
50
60
70
Angle 2θ (°)

Figure 5

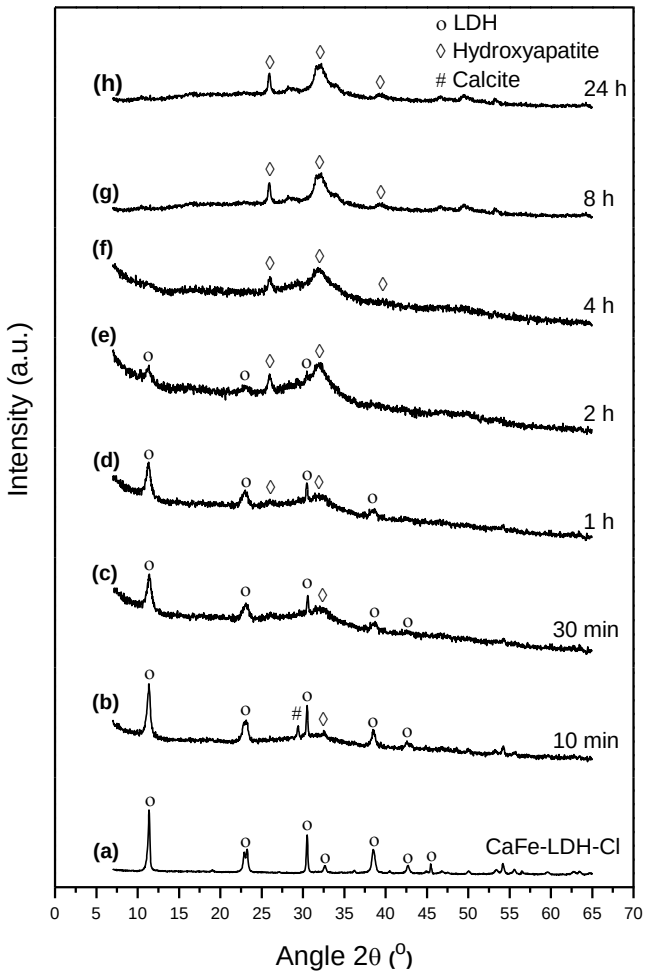
o LDH
◊ Hydroxyapatite
Calcite
(h)
24 h
(g)
8 h
(f)
4 h
(e)
2 h
(d)
1 h
(c)
30 min
(b)
10 min
(a)
CaFe-LDH-Cl
Intensity (a.u.)
0 5 10 15 20 25 30 35 40 45 50 55 60 65 70
Angle 2θ (°)

Figure 6

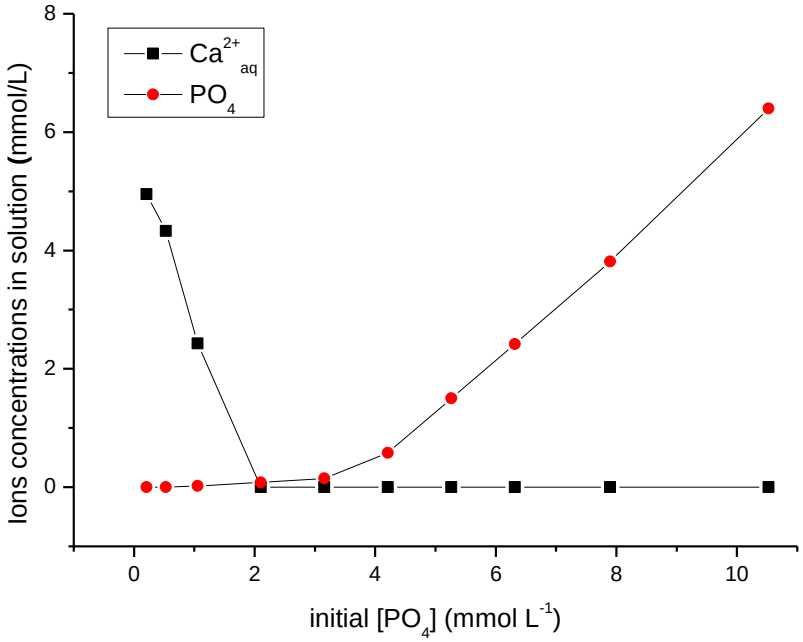
Ca2+ aq
PO4
Ions concentrations in solution (mmol/L)
initial [PO4] (mmol L-1)
0
2
4
6
8
10

Figure 7

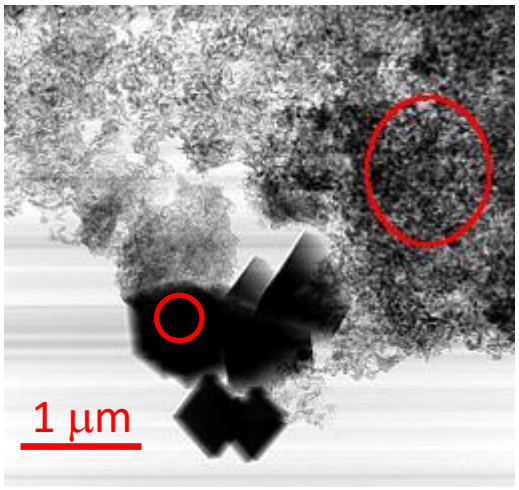

Figure 8

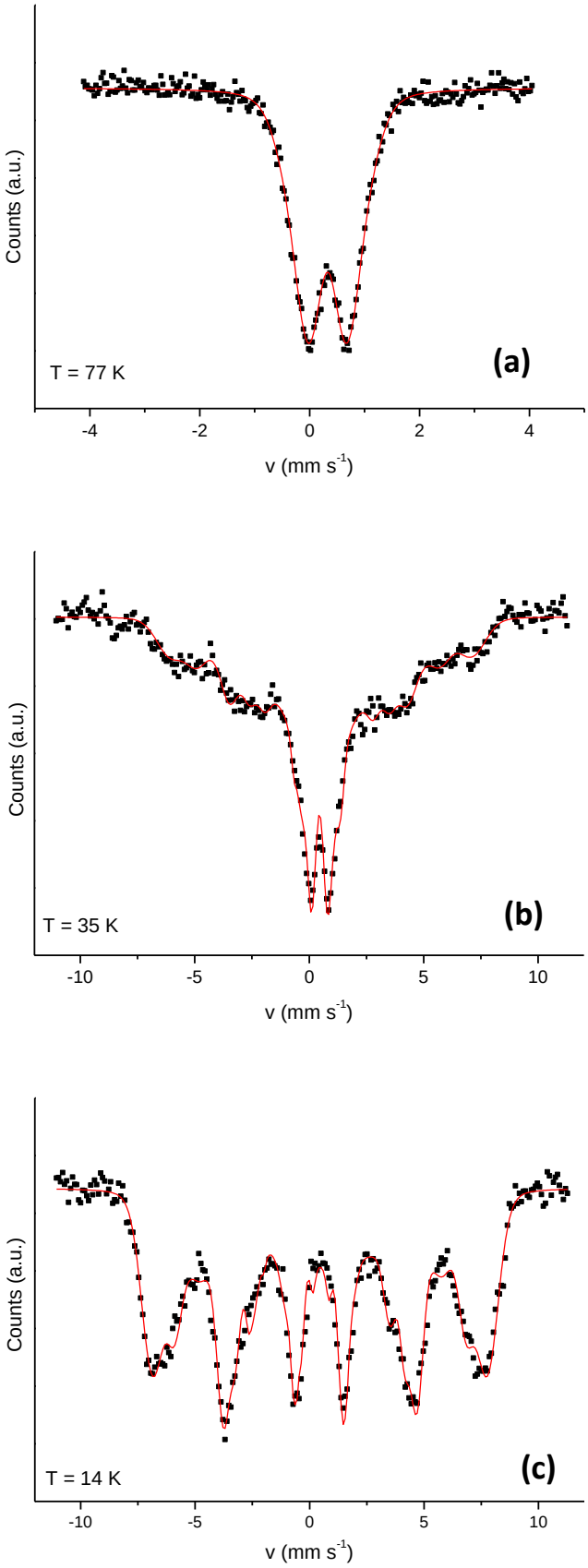
Counts (a.u.)
T = 77 K
(a)
-4
-2
0
2
4
v (mm s-1)
Counts (a.u.)
T = 35 K
(b)
-10
-5
0
5
10
v (mm s-1)
Counts (a.u.)
T = 14 K
(c)
-10
-5
0
5
10
v (mm s-1)

Figure 9

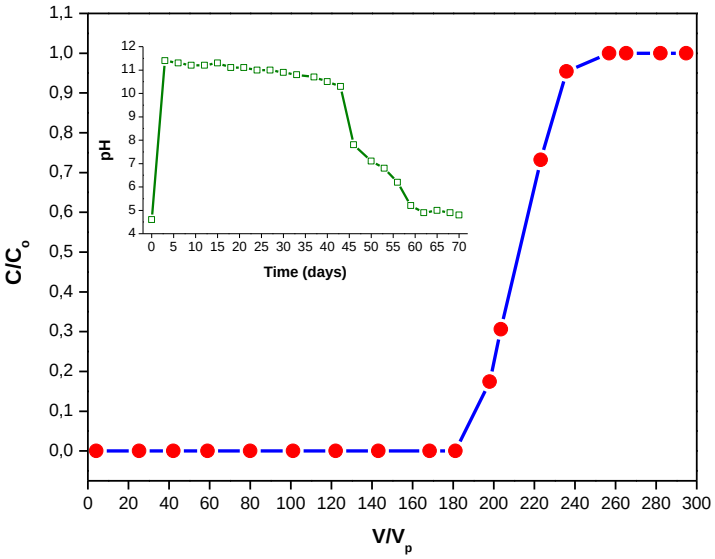

Figure 10

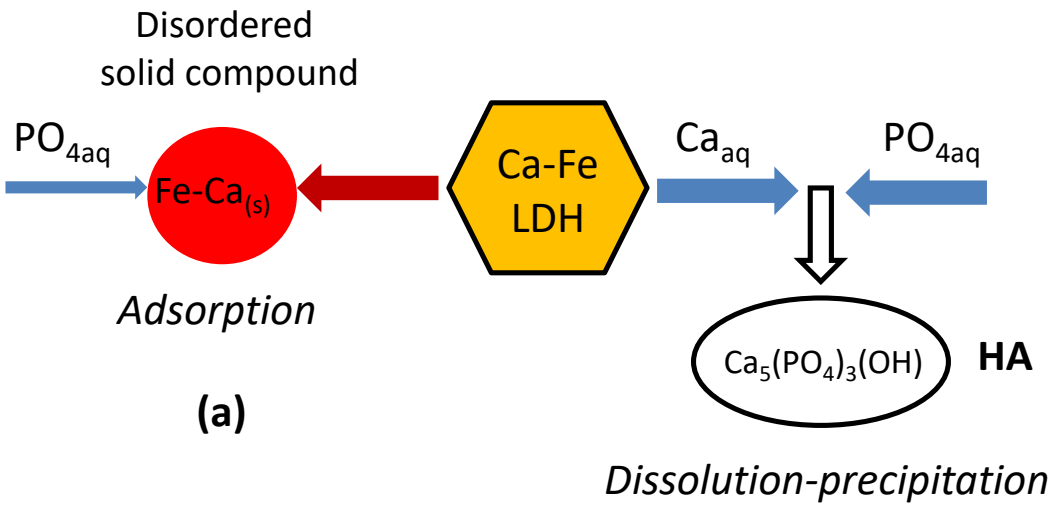
Disordered
solid compound
PO_{4aq}
Fe-$Ca_{(s)}$
Ca-Fe
LDH
Ca_{aq}
PO_{4aq}
Adsorption
$Ca_5(PO_4)_3(OH)$
HA
(a)
Dissolution-precipitation

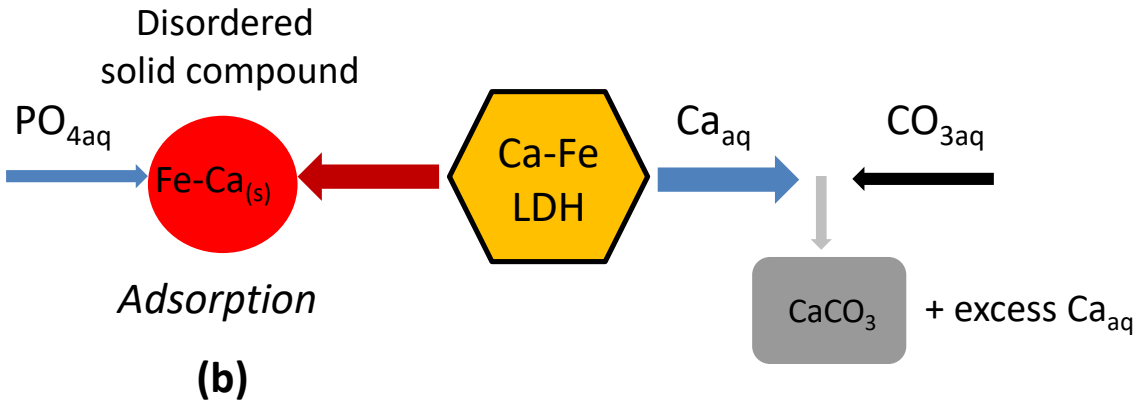
Disordered
solid compound
PO_{4aq}
Fe-$Ca_{(s)}$
Ca-Fe
LDH
Ca_{aq}
CO_{3aq}
Adsorption
$CaCO_3$
+ excess Ca_{aq}
(b)

Table 1

HDL type	$q_e^{(Max)}$ (mg P-PO_4 g^{-1}) (*)	$q_e^{(Max)}$ (mmol PO_4 g^{-1})	Initial [PO_4] (mg L^{-1})	LDH dose (g L^{-1})	pH	Ref.
Ca-Al-Cl	179	5.8	30-5400	2	4-7	Jia et al., 2016
Ca-Al-Cl	132	4.2	100-500	1	7-9	Qian et al., 2012
Ca-Al-Cl (synthesized from gastropod shell)	69	2.2	25-300	2	(**)	Oladoja et al., 2014
Ca-Al-NO_3	64	2	50-1000	10	8.1	Bekele et al., 2019)
Ca-Al-NO_3	66	2.15	~1- ~30	0.3	7	Ashekuzzaman et al., 2014
Ca-Mg-Al-NO_3	71	2.3	~1- ~30	0.3	7	Ashekuzzaman et al., 2014
Ca-Fe-NO_3	46	1.5	~1- ~30	0.3	7	Ashekuzzaman et al., 2014
Ca-Fe-Cl	~ 90	~2.9	60-300	0.4	(**)	Tsuji and Fujii, 2014
Ca-Fe-Cl	130	4.2	20-2000	1	7	This work

(*) The values reported for $q_e^{(Max)}$ are those corresponding to data obtained by using the fitting of the isotherm experiments (**) The pH values of the isotherm experiments were not provided.

Table 2

Region	Spot	O (at.%)	P (at.%)	Ca (at.%)	Fe (at.%)
1	A	61.1	5.6	22.4	10.9
	B	49.0	10.6	24.1	16.3
	C	59.6	-	40.4	-
2	D	56.8	5.8	24	13.4
	E	68.1	3.2	9	19.7
	F	59.9	-	40.1	-
3	G	61.6	5.7	22.5	10.2
	H	63.8	4.9	12.2	19.1

Table 3

Temp. (K)	Fig. Spectrum	Component	δ (mm s^{-1})	Δ or ε (mm s^{-1})	*H* (kOe)	*RA* (%)
77 K	Fig 8a	D_1	0.44	0.84	-	100
35 K	Fig 8b	D_1	0.45	0.71	-	13
		D_2	0.55	3.2	-	46
		S_1	0.42	0.02	256	10
		S_2	0.46	0.06	408	16
		S_3	0.43	-0.02	328	15
14 K	Fig 8c	D_1	0.76	1.99	-	10
		S_1	0.49	0.003	270	29
		S_2	-2.8	-0.46	133	3
		S_3	0.45	0	453	40
		S_4	0.46	0	394	18

δ :Isomer shift, Δ *or* ε **:** Quadrupole shift or quadrupole splitting, *H* : Hyperfine field, *RA* : Relative area of the component.

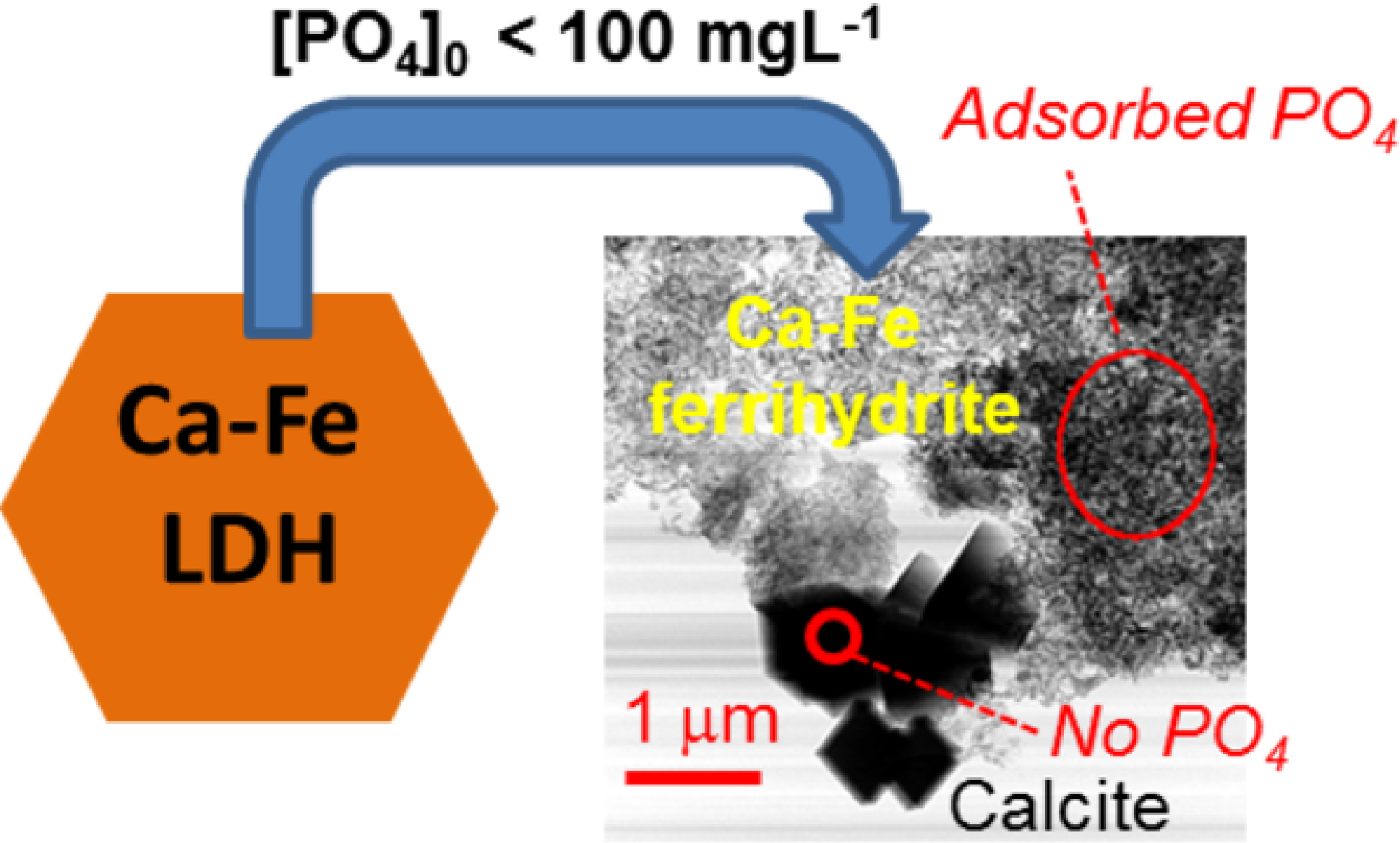
[PO4]0 < 100 mgL-1
Adsorbed PO4
Ca-Fe LDH
Ca-Fe ferrihydrite
1 µm
No PO4
Calcite